Journal of Solid State Chemistry 181 (2008) 2462–2468

Contents lists available at ScienceDirect

Journal of Solid State Chemistry

journal homepage: www.elsevier.com/locate/jssc

Electronic structures and optical properties of wurtzite type LiBSe$_2$ (B = Al, Ga, In): A first-principles study

Long-Hua Li [a,b], Jun-Qian Li [c], Li-Ming Wu [a,*]

[a] State Key Laboratory of Structural Chemistry, Fujian Institute of Research on the Structure of Matter, Chinese Academy of Sciences, Fuzhou, Fujian 350002, People's Republic of China
[b] Graduate School of the Chinese Academy of Sciences, Beijing 100039, People's Republic of China
[c] Department of Chemistry, Fuzhou University, Fuzhou, Fujian 350002, PR China

ARTICLE INFO

Article history:
Received 13 March 2008
Received in revised form
28 May 2008
Accepted 30 May 2008
Available online 7 June 2008

Keywords:
DFT
Wurtzite type selenides
Electronic structure
Band gap

ABSTRACT

The electronic structures of three wurtzite type isostructural compounds LiBSe$_2$ (B = Al, Ga, In) are studied by the density functional theory (DFT). The results reveal that the presence of Li cations has direct influence on neither the band gaps (Eg) nor the bonding levels, but plays an important role in the stabilization of the structures. The band structures and densities of states (DOS) are analyzed in detail, and the band gaps of LiBSe$_2$ adhere to the following trend $Eg_{(LiAlSe2)} > Eg_{(LiGaSe2)} > Eg_{(LiInSe2)}$, which is in agreement with the decrease of the bond energy of the corresponding Se 4p–B s antibonding orbitals. The role of the active s electrons of B element on the band gaps is also discussed. Finally, the optical properties are predicted, and the results would be a guide to understand the experiments.

1. Introduction

Ternary chalcogenides with the general formula $A^{I}B^{III}C_2$ (A = Li, Na, Cu, Ag; B = Al, Ga, In; C = S, Se, Te) are of considerable interest because of their potential optoelectronic applications as solar energy converters, nonlinear optical (NLO) devices, light emitting diodes (LED), and detectors [1]. Usually, these compounds belong to two crystallographic categories according to the identity of A cations. If A equals noble-metal cation (A = Cu, Ag), the compound adopts chalcopyrite structure (diamond-like or $CuFeS_2$ type; space group $I\bar{4}2d$; point group $\bar{4}2m$). If A equals alkali metal (A = Li, Na), the compound crystallizes in orthorhombic α-$NaFeO_2$ type (orthorhombic $Pna2_1$; point group $mm2$), a modification of wurtzite type. These three-dimensional networks are both constructed by tetrahedral units via sharing four corners only differ in the stacking sequences of the anions. The chalcopyrite type is a zinc-blende superstructure in which C atoms have an *fcc* packing, and the orthorhombic type is a wurtzite superstructure in which C atoms are *hcp* stacked [1,2]. The cationic noble-metal (A = Cu, Ag) or alkali metal (A = Li, Na) provides electron to the corresponding anionic framework; meanwhile, it may participate in constructing the band structure. Relatively, the alkali metal (A = Li, Na) is merely an electron donator and hardly contributes to the frontier orbitals because of the small ion radius and simple extra nuclear electron configuration. Thus, the Li- or Na-analogues will show less cation effect on the electronic structures.

Recently, most reports are focused on the chalcopyrite type Cu- or Ag-analogues in $A^{I}B^{III}C_2$ families. However, the chalcopyrite is structurally uniaxial and therefore bears some limitations in thermal properties [3], such as low thermal conductivity and lager coefficient of thermal expansion anisotropy. For example, $AgGaS_2$ and $AgGaSe_2$ [4] would be perfect materials for the nonlinear optical applications in the mid-infrared region, owing to the birefringence, transparence and large nonlinear coefficient. Nevertheless, their negative thermal expansion coefficient along the optical axis and low thermal conductivity lead to the undesired formations of the typical stresses and the microtwin [4] defects.

In order to avoid these drawbacks, the wurtzite type Li-analogues, LiBC_2 (B = Al, Ga, In; C = S, Se, Te), seem to be good candidates with the following considerations: (1) the biaxial characteristic of LiBC_2 suggests the existence of the optical propagation directions which are thermally insensitive; (2) the band gaps of LiBC_2 are always larger than those of the $AgBC_2$ or $CuBC_2$ [5–7]; (3) the bonding and optical properties of LiBC_2 are insensitive to the hybridization between d orbitals of the cation and p states of the anion (because Li^+ has no d orbitals)—in contrast to that of the Cu- or Ag-analogues; (4) the substitution of Ag ions by the lighter Li ions increases both the frequencies of the crystal lattice vibrations, Debye temperature, and the laser damage threshold [4].

* Corresponding author.
E-mail address: liming_wu@fjirsm.ac.cn (L.-M. Wu).

0022-4596/$ - see front matter © 2008 Elsevier Inc. All rights reserved.
doi:10.1016/j.jssc.2008.05.047

Up to date, the available experimental data of LiBSe$_2$ are limited on bond parameters [1,5,6,8], thermal [3,7,9,10], optical properties [11–13], and structural phase transitions [14], and none theoretical study on the electronic structure and optical properties has been done.

In this paper, we present the first-principles calculations of the electronic structures and the optical properties of LiBSe$_2$ (B = Al, Ga, In). The program, the calculation methods and the crystal structures are described in Section 2. The analyses of the band structures and optical properties are presented in Section 3, and the last section is conclusion.

2. Computational details

2.1. Computational method

A density functional theory (DFT) code Wien2k [15] was used to calculate the electronic structures and the optical properties, which is an implementation of a hybrid full potential (linear) augmented plane-wave plus local orbital (L/APW+lo) [16] method. The Perdew–Burke–Ernzerhof generalized gradient approximation (PBE-GGA) [17] was used for the exchange-correlation potentials. The muffin-tin (MT) radius was set to be 2.32, 2.20, 2.30, 2.38 and 2.22 for Li, Al, Ga, In and Se, respectively. A plane-wave expansion with $R_{MT} \times K_{MAX}$ equals to 8, G_{MAX} is 14 and k sampling with 48 k-points in the first Brillouin zone turns out to be enough. The self-consistent calculations are converged only when the total energy converges to less than 10^{-4} Ry. The electronic configurations for Li, Al, Ga, In and Se are Li: [He] $2s^1$, Al: [Ne] $3s^23p^1$, Ga: [Ar] $3d^{10}4s^24p^1$, In: [Kr] $4d^{10}5s^25p^1$, and Se: [Ar] $3d^{10}4s^24p^4$, respectively. In the optical properties calculations, 336 k points were considered in the first Brillouin zone.

Castep [18] employing the DFT plane-wave pseudopotentials method was also used for comparison. The electronic properties were calculated using the generalized gradient approximation (GGA) with gradient corrected functional PBE. Ultrasoft pseudopotentials (USP) [19] were applied with a plane wave cutoff energy of 350 eV. The valence electronic configurations for Li, Al, Ga, In and Se are $1s^22s^1$, $3s^23p^1$, $3d^{10}4s^24p^1$, $4d^{10}5s^25p^1$ and $4s^24p^4$, respectively. A $4 \times 3 \times 4$ k-points mesh was used in the band structure calculations. The k integration over the Brillouin zone was performed using the Monkhorst–Pack mesh. Norm-conserving pseudopotentials (NCP) [20] were used to compare the results of the band gap. All geometric structures were optimized via employing Castep at GGA-PBE theory level. Under the restriction of the given symmetry, the total energy was minimized via varying the cell parameters and the atomic positions to obtain the structure optimization. All forces on the atoms were converged to less than 0.01 eV/Å, and the total stress tensor was reduced to 0.02 GPa by using the BFGS algorithm. The calculated total energy converged to less than 10^{-6} eV/atom.

2.2. Crystal structure of LiBSe$_2$

A primitive orthorhombic unit cell of LiBSe$_2$ (Fig. 1a) was built by four Li atoms, four B (B = Al, Ga or In) atoms and eight Se atoms with a C_{2v}^9 symmetry ($Pna2_1$ space group). A glide plane is normal to [010] axis with 1/2 lattice vector along the a-axis, and a "diagonal" glide plane is normal to the [100] direction. A twofold 2_1 screw axis is along the c-axis. All atoms occupy the 4a Wyckoff sites. The B cation is surrounded by four Se anions in a distorted tetrahedral geometry. Each Se anion is bonded with two Li cations and two B cations, The optimized lattice constants with DFT for LiAlSe$_2$ are a = 6.852 Å, b = 8.291 Å, and c = 6.537 Å, which are close to the experimental values (a_{exp} = 6.823 Å, b_{exp} = 8.266 Å and c_{exp} = 6.524 Å from ICSD #280225) with a deviation less than 0.5%. The other two sets are a = 6.911 Å, b = 8.392 Å, and c = 6.622 Å for LiGaSe$_2$; a = 7.348 Å, b = 8.605 Å, and c = 6.933 Å for LiInSe$_2$, respectively. Both are comparable to the experimental ones: LiGaSe$_2$, (a_{exp} = 6.832 Å, b_{exp} = 8.237 Å, and c_{exp} = 6.535 Å) from ICSD #96915 and LiInSe$_2$, (a_{exp} = 7.183 Å, b_{exp} = 8.398 Å, and c_{exp} = 6.781 Å) from ICSD #60838.

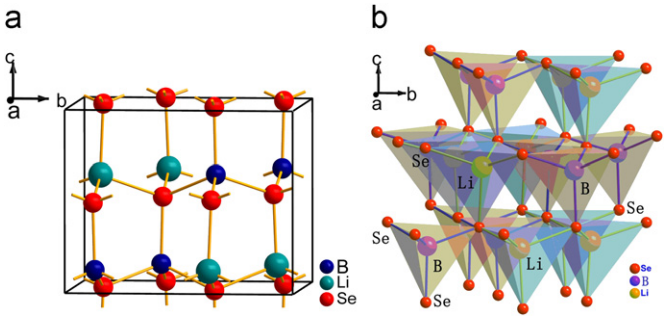

Fig. 1. (a) Schematic diagram of the LiBSe$_2$ unit cell. (b) The stacking structure of BSe$_4$ and LiSe$_4$ tetrahedral view along the a-axis.

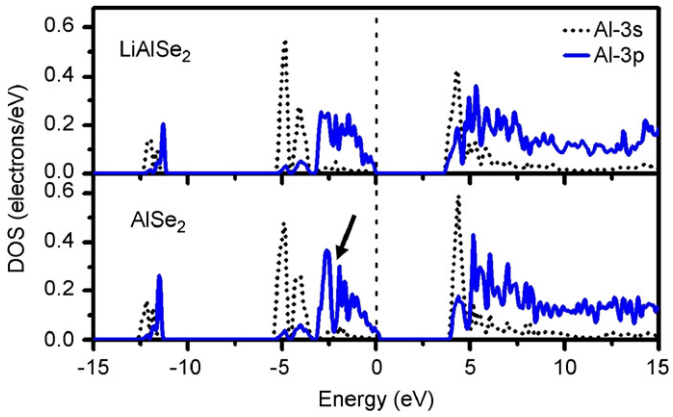

Fig. 2. Partial density of states of Al in two models. A slight split is indicated by an arrow. The Fermi energy is set to 0 eV.

The 3D network structure of LiBSe$_2$ is constructed by the vertex-sharing BSe$_4$ and LiSe$_4$ tetrahedra (Fig. 1b). The *hcp* packing of Se anions generates the tetrahedral and octahedral interstices. Li or B cations occupy half of the tetrahedral holes, and all the octahedral interstices are empty.

3. Results and discussion

3.1. Electronic properties

3.1.1. Roles of Li cations

LiAlSe$_2$ is chosen as a representative to understand the role of Lithium in LiBC_2 compounds. Two models have been designed: regular $Li_4Al_4Se_8$ lattice (model-**1**) and Al_4Se_8 (model-**2**). Note that four electrons have been added to Al_4Se_8 during the calculations for better comparison with that of model-**1**.

The partial densities of states (PDOS) of both models are plotted in Fig. 2. In model-**2**, Al-3s valence bands (dotted line) locate in two regions from about −12.60 to −11.39 eV and from −5.48 to −3.31 eV. The sharp curves indicate that Al-3s orbitals are relative localized. Al-3p valence states (solid line) are mainly located from −12.51 to −10.7 eV and −5.71 to 0 eV. The PDOS of Se atoms are presented in Fig. 3, the states from −12.70 to −11.26 eV

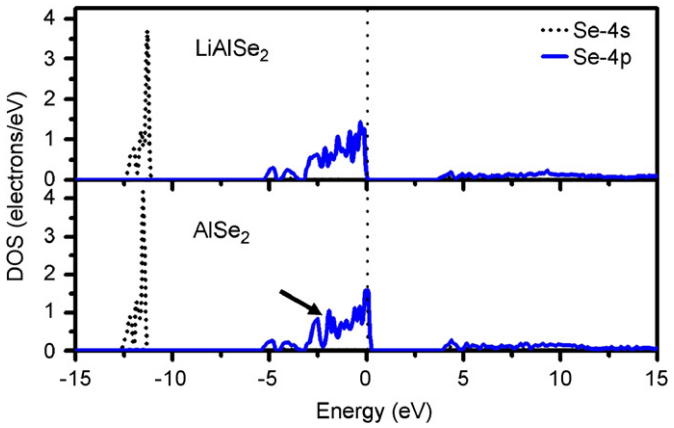

Fig. 3. Partial density of states of Se in two models. The dashed line denotes the Fermi energy.

are mainly form the Se-4*s* valence bands, the sharp curves also indicate the localization character of Se-4*s* orbitals. As shown in both Figs. 2 and 3, the components of the states from −3.14 to 0 eV are mainly Se-4*p* valence states and Al-3*p* states. The wide distributions of Al-3*p* and Se-4*p* indicate a long-range delocalization effect of these *p* electrons.

The calculated DOS of model **1** and **2** are nearly identical as shown in Fig. 2 and 3, which suggests that the existence of Li cations has no significant influence on the states of Al and Se. But the Fermi energy of two models are different, 1.95 eV for $LiAlSe_2$ and 1.13 eV for $AlSe_2$, respectively. In case of $LiAlSe_2$, more electrons are available to fill the valence bands below Fermi level, while in $AlSe_2$, the conduct states move slightly towards higher energy. As a result, the existence of Li lowers the ground energy and thus stabilizes the structure.

A difference has been seen between two models **2**, as indicated by an arrow in Figs. 2 and 3, that both Se-4*p* and Al-3*p* states have a small split (around −2.46 eV). The reason is considered as followed: The formation of $[LiSe_4]$ tetrahedron in $LiAlSe_2$ suggests Li ions should have some direct influences on Se ions. Whereas the Li–Al distance is 4.133 Å in average, too long for a reasonable bond distance, so Li–Al contact only has a secondary interaction and merely affects the long-range interactions. On the other hand, the tetrahedral Se in $LiAlSe_2$ ($[SeAl_2Li_2]$) constructed by two Al and two weakly bonded Li, has been changed to $[SeAl_2]$ planar triangle with the absence of Li in model **2**. That is to say, the dispersion of Se-4*p* electrons in both model **1** and **2** ($[SeAl_2Li_2]$ vs. $[SeAl_2]$) over two Al–Se bonds should be similar, only differs in that some of the Se-4*p* electrons are more localized in model **2** without the influence of Li–Se bonds. As mentioned above, both the Al-3*p* and Se-4*p* electrons have a long-range delocalization effect, so a split of Al-3*p* has been also seen (at about −2.46 eV) in model **2**, hence, Li cations have some impacts on the delocalization of Se-4*p* and Al-3*p* electrons.

3.1.2. DOS of $LiBSe_2$

As shown in Fig. 4a–c, the trivial PDOS contribution of Li suggests its negligible influence around the Fermi levels. The *d* states of Ga or In are fully filled and highly localized, and the bonding levels of *d* states should also be ignored. According to the deformed tetrahedral crystal field, *d* states are split into *e* and t_2 parts ($LiGaSe_2$ shown in Fig. 4b and $LiInSe_2$ in Fig. 4c), which are highly localized at the energy range of −14.52 to −13.70 eV and −12.75 to −10.92 eV, respectively. Note that no Al-*d* electron has been considered in the calculations of $LiAlSe_2$.

As shown in Fig. 4a–c, the PDOSs of *B* are similar around Fermi level (*B* = Al, Ga, In). The majority of HOCO (highest occupied

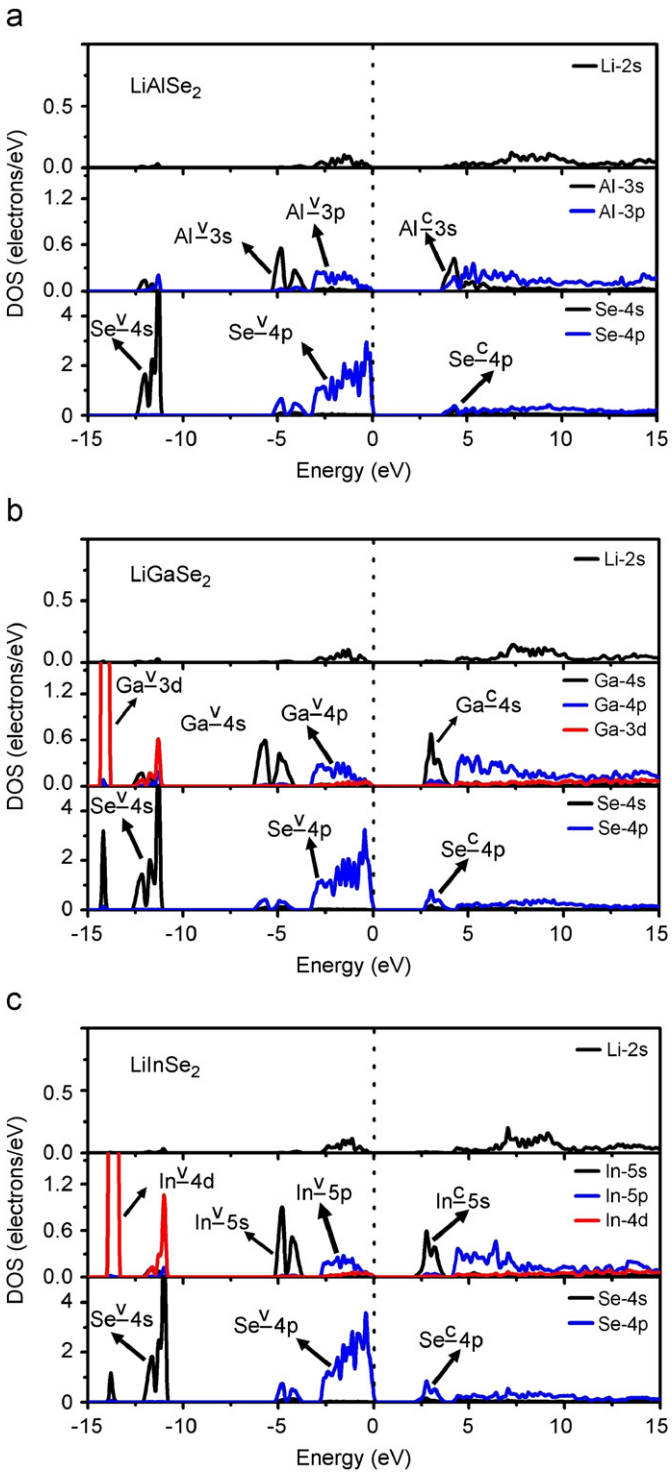

Fig. 4. Density of states of (a) $LiAlSe_2$, (b) $LiGaSe_2$ and (c) $LiInSe_2$. Fermi level is set to zero. The symbol 'v' and 'c' represents valence states and conduction states, respectively.

crystal orbitals) is constructed by the Se-4*p* as a dominant component and *B*-*p* (i.e., Al-3*p*, Ga-4*p* or In-5*p*). Therefore, the HOCO of three compounds has no significant difference. The LUCO (lowest unoccupied crystal orbitals) is mostly the antibonding orbitals of *B*-*s* and Se-4*p*. Because the different energy level of *B*-*s* states (the energy sequence of *B*-*s*: Al-3*s* < Ga-4*s* < In-5*s*), the band gaps of these compounds are different as discussed as followed.

3.1.3. Band structures of $LiBSe_2$

The band structures of $LiBSe_2$ (B = Al, Ga, In) are similar as shown in Fig. 5a–c. We present the detailed description on $LiAlSe_2$ as example. The HOCO comes from σ_{p-p} interaction between Se-4p_z and Al-3p_z (Ga-4p_z, In-5p_z in other two cases) in the energy range of −3.25 eV to Fermi level (0 eV), and the corresponding $(\sigma_{p-p})^*$ antibonding orbitals locate above 4.64 eV. The bands dispersing from −5.40 to −3.31 eV are constructed by selenium 4p–aluminum s. And the LUCO in the range of 3.28–4.63 eV is constituted by the antibonding orbitals of (selenium 4p–alumimetry (C_{2v}^9) of the structure, the band degeneration occurs between Γ and Z. Since the maximum of HOVB (highest occupied valence bands) and the minimum of LUCB (lowest unoccupied conduction bands) both occur at Γ point, $LiBSe_2$ is a direct semiconductor.

As described above, $LiBSe_2$ (B = Al, Ga, In) are direct band gap semiconductors and the band gap values are somewhat determined by the energies of the conduction bands. The shift of the energies of selenium 4p–B s bands (colored lines) is obvious in Fig. 5, which indicates that B-s bands are important in

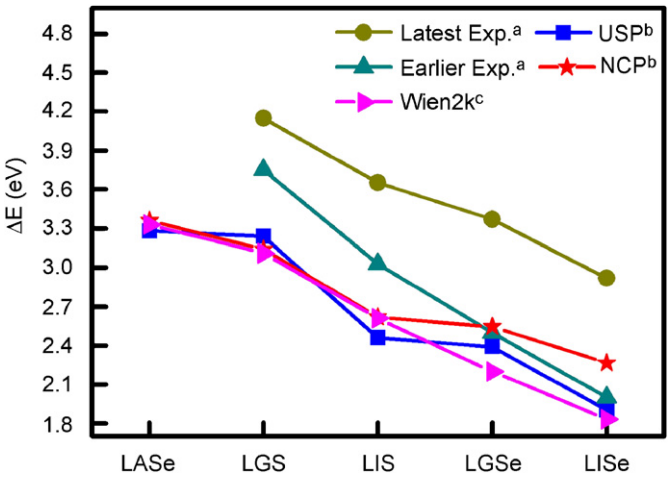

Fig. 6. The band gaps of $LiBC_2$. L, A, G, and I represent Li, Al, Ga and In, respectively. [a]: values taken from reference 13; [b]: values calculated by Castep; [c]: values calculated by Wien2k.

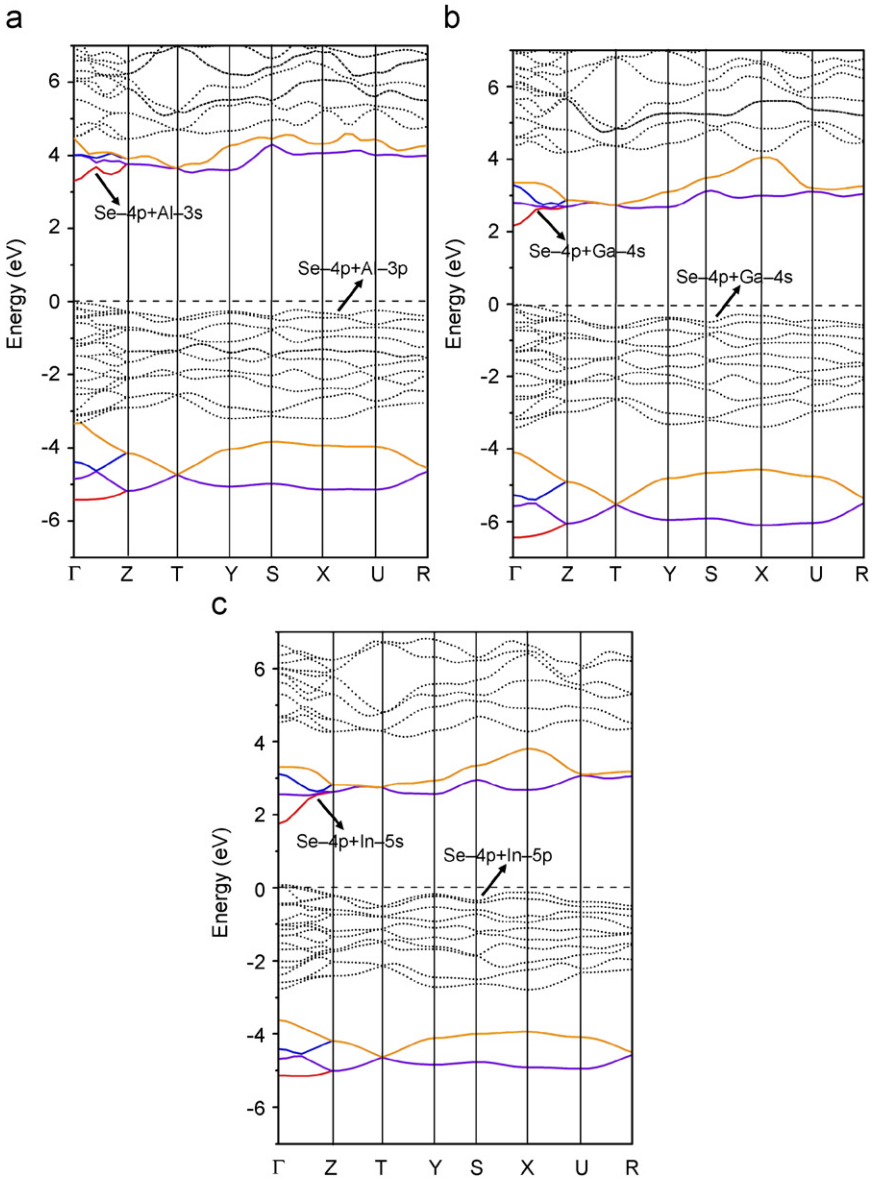

Fig. 5. Band structures of (a) $LiAlSe_2$, (b) $LiGaSe_2$ and (c) $LiInSe_2$. The Brillouin zone for a primitive orthorhombic cell: Γ = (000); $Z = (00\frac{1}{2})$; $X = (0\frac{1}{2}0)$; $Y = (-\frac{1}{2}00)$; $T = (-\frac{1}{2}0\frac{1}{2})$; $U = (0\frac{11}{22})$; $S = (-\frac{11}{22}0)$; $R = (-\frac{111}{222})$. The dashed line denotes the Fermi energy.

determining the band gaps of Li*B*Se$_2$. In fact, the metallicity of IIIA-group element increases from Al to In, naturally, the conduction bands decrease in energy with the increase of the metallicity of the *B*–Se bond. That is to say, with the decrease of the electronegativity of *B*, the energy of selenium 4*p*–*B s* antibonding level decreases. So does the band gap.

While for the related sulfides Li*B*S$_2$, the electronegativity of sulfur is stronger than that of selenium, so the HOCO of Li*B*S$_2$ locates at lower energy than that of Se-analogues. And the corresponding LUCO constructed by the sulfur 3*p*–*B s* antibonding orbitals appears at higher energy. Thus, the band gaps of Li*B*S$_2$ should be wider. The recent experimental results by Isaenko and coworkers are consistent with our calculations, for example the band gaps of LiGaS$_2$ (3.75 eV) and LiInS$_2$ (3.03 eV) [13] are remarkably larger than that of LiGaSe$_2$ (2.51 eV), and LiInSe$_2$ (2.00 eV) [13].

The comparison between the calculated and experimental band gaps are shown in Fig. 6. In general, the sulfides have wider

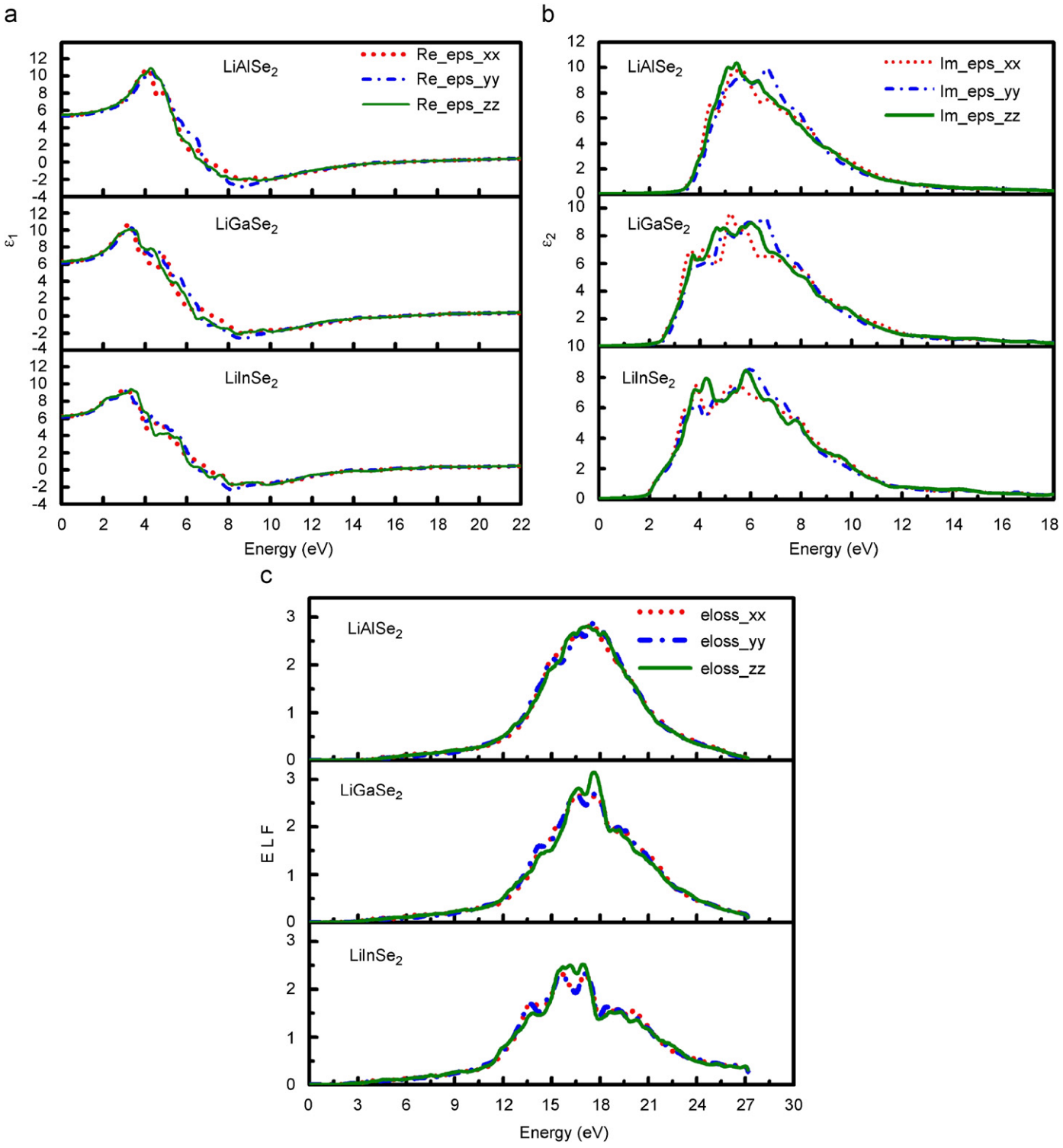

Fig. 7. (a) Real part ε_1 vs. *E* (energy) in Li*B*Se$_2$ (*B* = Al, Ga, In). (b) The corresponding imaginary part of Li*B*Se$_2$. (c) Energy loss function (ELF) of Li*B*Se$_2$.

band gaps than the corresponding selenides. And both sets of values decrease with the increase of the metallicity of *B* as discussed above. Our USP calculated band gaps for $LiAlSe_2$, $LiGaSe_2$, $LiInSe_2$, $LiGaS_2$ and $LiInS_2$ are 3.28, 2.39, 1.9, 3.24, and 2.46 eV, respectively. These are in agreement with the results calculated by Wien2k and Castep. The calculated and experimental band gap values follow the same descend trend, and the systematic discrepancy between them could be understood in two ways: (1) the unavoidable disorder and defects in a real crystal affect significantly the measured band gap values; (2) GGA is well known to underestimate the band gap. The NCP gives larger band gap values for all compounds except for $LiGaS_2$, which implies that the improvement of the calculation method could give better estimation.

3.2. Optical properties

The calculated imaginary part $\varepsilon_2(w)$ of the complex dielectric function $\varepsilon(w) = \varepsilon_1(w)+i\varepsilon_2(w)$ was separated into two components, i.e., $\varepsilon_{2xx/yy}(w)$ and $\varepsilon_{2zz}(w)$, that are the average polarization of the spectra perpendicular and parallel to the *c*-axis, respectively. The imaginary part can be obtained by using the Kubo–Greenwood formula [21] and the real part is deduced from the imaginary value via Kramers–Kronig relation [22].

The real part of the dielectric function $\varepsilon_1(w)$ and the imaginary part $\varepsilon_2(w)$ are plotted in Fig. 7a and b, in an energy range of 0.0–22.0 eV, respectively. The imaginary part $\varepsilon_2(w)$ of the dielectric function is associated with the interband transitions, where the intraband transitions are ignored because only in metallic materials the intraband transitions are considered [23]. As shown in Fig. 7a, the band locates around 4.23 eV in $LiAlSe_2$ is attributed to the interband transitions from selenium 4*p* valence bands to aluminum 3*s* conduction bands. The differences between the dispersion of the function ε_{xx}, ε_{yy}, and ε_{zz} are correlated to the anisotropy of the crystal. And the analyses give similar results for $LiGaSe_2$ and $LiInSe_2$. The down shift of the first peak in energy (Fig. 7a) may reflect the reduction of band gaps. The Optical dielectric constant of $LiAlSe_2$, $LiGaSe_2$ and $LiInSe_2$ are given in Table 1. Note that the calculations are carried out for a perfect static crystal at 0 K and no zero-point vibration is involved, while the experimental data are obtained at room temperature under which the effects of vibration are not ignorable.

The energy loss function (ELF) is obtain from the dynamic dielectric constant and is proportional to $\mathrm{Im}(-1/\varepsilon_w)$ (Fig. 7c). And the ELF is comparable to the spectroscopic data, such as parallel electron energy loss spectroscopy (PEELS) [24], which give the information on bonding and electronic properties through the information of the interaction between the sample and the electron beam. Unfortunately, the related spectroscopic data are insufficient at present. A significant feature of the ELF spectrum (in the energy region up to 50.0 eV) is the plasmon peak, which shows the collective excitation of the loosely bound valence electrons into the unoccupied energy levels in the conduction bands. In principle, the intensity of the spectrum is related to the dielectric function and the interband transitions according to the dielectric theory.

As shown in Fig. 7c, a broad peak spans from 3.00 to 24.00 eV. The plasmon energy at the peak maximum is 17.29 eV (eloss_*zz*), 17.64 eV (eloss_*zz*) and 16.94 eV (eloss_*zz*) for $LiAlSe_2$, $LiGaSe_2$ and $LiInSe_2$, respectively. Since the lack of experimental values of the ELF data, a direct evaluation of our theoretic results is unavailable. Such calculations may stimulate the experimental investigations.

Table 1
Optical dielectric constant of $LiAlSe_2$, $LiGaSe_2$ and $LiInSe_2$

	$LiAlSe_2$		$LiGaSe_2$		$LiInSe_2$	
	Cal.	Exp.	Cal.	Exp.	Cal.	Exp.
ε_{1xx}	5.43	–	6.29		6.24	
ε_{1yy}	5.36		6.17		6.18	
ε_{1zz}	5.48		6.33		6.28	
$\bar{\varepsilon}$	5.42		6.26	8.10[a]	6.23	7.59[a]

[a] From Ref. [6]. Cal. and Exp. represent calculation and experiment, respectively.

4. Conclusion

In this paper, the band structures, densities of states (DOS) as well as the roles of Li cations of three isostructural selenides $LiBSe_2$ (B = Al, Ga, In) are discussed on the basis of the DFT study. Except for stabilizing the structures, Li cations also put some effects on the delocalization of selenium 4*p* and *B*-*p* electrons, but barely participate in the bonding levels of $LiBSe_2$. This implies that the simple replacement of the Li cations with other alkali metals is not a sufficient way to tune the electronic properties of $LiBSe_2$ derivatives, two possible ways are (1) to change the stacking pattern of anionic building unit $[BSe_2]^-$; (2) doping in the $[BSe_2]^-$ framework either at Se sites with other chalcogen elements (S or Te) or *B* sites with different combinations with Al, Ga and In.

The calculated band gaps are typical sp^3 hybrid band gap [25], which are influenced by the electronegativity of *B* elements. The band gaps follow the trend of $LiAlSe_2 > LiGaSe_2 > LiInSe_2$, which agrees with the energy sequence of the antibonding level between selenium 4*p* and *B*-*s* orbitals, that is $Se_{(4p)}$–$Al_{(3s)} > Se_{(4p)}$–$Ga_{(4s)} > Se_{(4p)}$–$In_{(5s)}$.

The calculated dielectric constants (Table 1) by Wien2k are smaller than the experimental values. Such discrepancy may be caused by the exclusion of the atomic vibrations in the calculations. And the predictions of the plasmon energy of $LiBSe_2$ are available for the evaluation by the experiments. More experimental measurements are under expectation.

Acknowledgments

This research was supported by the National Natural Science Foundation of China under Projects (20401014, 20773130, 20521101), NSF of Fujian Province (2005HZ01-1) and the "Key Project from CAS" (KJCX2-YW-H01).

References

[1] J.Y. Kim, T. Hughbanks, Inorg. Chem. 39 (2000) 3092–3097.
[2] L. Isaenko, A. Yelisseyev, S. Lobanov, A. Titov, V. Petrov, J.J. Zondy, P. Krinitsin, A. Merkulov, V. Vedenyapin, J. Smirnova, Cryst. Res. Technol. 38 (2003) 379–387.
[3] A.P. Yelisseyev, V.A. Drebushchak, A.S. Titov, L.I. Isaenko, S.I. Lobanov, K.M. Lyapunov, V.A. Gruzdev, S.G. Komarov, V. Petrov, J.J. Zondy, J. Appl. Phys. 96 (2004) 3659–3665.
[4] L. Isaenko, A. Yelisseyev, S. Lobanov, V. Petrov, F. Rotermund, G. Slekys, J.J. Zondy, J. Appl. Phys. 91 (2002) 9475–9480.
[5] K. Kuriyama, T. Nozaki, J. Appl. Phys. 52 (1981) 6441–6443.
[6] T. Kamijoh, T. Nozaki, K. Kuriyama, J. Appl. Phys. 53 (1982) 761–763.
[7] O. Bidault, S. Fossier, J. Mangin, P. Strimer, A. Yelisseyev, L. Isaenko, S. Lobanov, Solid State Commun. 121 (2002) 207–211.
[8] P. Lawaetz, Phys. Rev. B 5 (1972) 4039–4045.
[9] T. Kamijoh, K. Kuriyama, J. Appl. Phys. 52 (1981) 1102–1103.
[10] E. Gmelin, W. Honle, Thermochim. Acta 269/270 (1995) 575–590.
[11] K. Kuriyama, T. Kato, A. Takahashi, Phys. Rev. B 46 (1992) 15518–15519.
[12] V. Petrov, A. Yelisseyev, L. Isaenko, S. Lobanov, A. Titov, J.J. Zondy, Appl. Phys. B: Lasers Opt. 78 (2004) 543–546.
[13] L. Isaenko, A. Yelisseyev, S. Lobanov, P. Krinitsin, V. Petrov, J.J. Zondy, J. Non-Cryst. Solids 352 (2006) 2439–2443.

[14] H.J. Beister, S. Ves, W. Honle, K. Syassen, G. Kuhn, Phys. Rev. B 43 (1991) 9635–9642.
[15] P. Blaha, K. Schwarz, G.K.H. Madsen, D. Kvasnicka, J. Luitz, WIEN2k, an augmented plane wave plus local orbitals program for calculating crystal properties,Vienna University of Technology, 2001.
[16] K. Schwarz, P. Blaha, G.K.H. Madsen, Comput. Phys. Commun. 147 (2002) 71–76.
[17] J.P. Perdew, K. Burke, M. Ernzerhof, Phys. Rev. Lett. 77 (1996) 3865–3868.
[18] M.D. Segall, P.J.D. Lindan, M.J. Probert, C.J. Pickard, P.J. Hasnip, S.J. Clark, M.C. Payne, J. Phys.: Condens. Matter 11 (2002) 2717–2744.
[19] D. Vanderbilt, Phys. Rev. B 41 (1990) 7892–7895.
[20] D.R. Hamann, M. Schlüer, C. Chiang, Phys. Rev. Lett. 43 (1979) 1494–1497.
[21] H. Jin, G.L. Zhao, D. Bagayoko, J. Appl. Phys. 101 (2007) 0331231–0331234.
[22] S. Laksari, A. Chahed, N. Abbouni, O. Benhelal, B. Abbar, Comput. Mater. Sci. 38 (2006) 223–230.
[23] H.Y. He, R. Orlando, M.A. Blanco, R. Pandey, E. Amzallag, I. Baraille, M. Rerat, Phys. Rev. B 74 (2006), 195123(1–8).
[24] K.X. Hu, I.P. Jones, J. Phys. D: Appl. Phys. 38 (2005) 183–187.
[25] N.E. Christensen, S. Satpathy, Z. Pawlowska, Phys. Rev. B 36 (1987) 1032–1050.